

Influences of accreting primordial black holes on the global 21 cm signal in the dark ages

Yupeng Yang ^{*}

School of Physics and Physical Engineering, Qufu Normal University, Qufu, Shandong, 273165, China

12 November 2021

ABSTRACT

Baryonic matter can be accreted on to primordial black holes (PBHs) formed in the early Universe. The radiation from accreting PBHs is capable of altering the evolution of the intergalactic medium (IGM), leaving marks on the global 21 cm signal in the dark ages. For accreting PBHs with mass $M_{\text{PBH}} = 10^3(10^4) M_{\odot}$ and mass fraction $f_{\text{PBH}} = 10^{-1}(10^{-3})$, the brightness temperature deviation $\Delta\delta T_b$ reaches ~ 18 (26) mK at redshift $z \sim 90$ ($\nu \sim 16$ MHz), and the gradient of the brightness temperature $d\delta T_b/d\nu$ reaches ~ 0.8 (0.5) mK MHz⁻¹ at frequency $\nu \sim 28$ MHz ($z \sim 50$). For larger PBHs with higher mass fraction, the brightness temperature deviation is larger in the redshift range $z \sim 30 - 300$ ($\nu \sim 5 - 46$ MHz), and the gradient is lower at the frequency range $\nu \sim 20 - 60$ MHz ($z \sim 23 - 70$). It is impossible to detect these low frequency radio signals from the Earth due to the influence of the Earth's ionosphere. However, after taking care of the essential factors properly, e.g. the foreground and interference, future radio telescope in lunar orbit or on the farside surface of the Moon has a chance of detecting the global 21 cm signals impacted by accreting PBHs and distinguishing them from the standard model.

Key words: cosmology:dark matter

1 INTRODUCTION

As a main component of the Universe, the existence of dark matter (DM) has been confirmed by many astronomical observations, but its nature still remains mysterious (Jungman et al. 1996; Bertone et al. 2005). Many DM models have been proposed and the most studied is that of weakly interacting massive particles (WIMPs). On the other hand, no detection of WIMPs has rekindled the interest in other DM models such as primordial black holes (PBHs), especially for the recent successful detection of gravitational waves possibly caused by the mergers of PBHs (Bird et al. 2016; Kohri & Terada 2021; De Luca et al. 2021a,b; Carr et al. 2020).

PBHs can form in the early Universe through the collapse of the large density perturbation. PBHs with masses $M_{\text{PBH}} \lesssim 10^{-16} M_{\odot}$ can emit different kinds of particles via Hawking radiation (Carr et al. 2010; Page 1977, 1976b,a). Due to the interactions between the particles emitted from PBHs and those existing in the Universe, the evolution of the intergalactic medium (IGM) can be changed through the effects of ionizing, heating, and excitation. PBHs with masses $M_{\text{PBH}} \gtrsim 10 M_{\odot}$ can also radiate high energy-

photons in the process of accreting baryonic matter on to them, and this radiation can also affect the evolution of the IGM. The changes of the evolution of IGM will be reflected in relevant astronomical observations, such as the anisotropy of the cosmic microwave background (CMB) and the global 21 cm signal (Yang 2019, 2018; Clark et al. 2018; Ricotti et al. 2008; Cang et al. 2021b; Poulin et al. 2017; Ali-Haïmoud & Kamionkowski 2017; Tashiro & Sugiyama 2013; Villanueva-Domingo & Ichiki 2021; Ünal et al. 2021).

Recently, the Experiment to Detect the Global Epoch of Reionization Signature (EDGES) reported the observation of the global 21 cm signal, showing an absorption feature with an amplitude $T_{21} \sim 500$ mK centered at redshift $z \sim 17$. The maximum amplitude observed is about twice as larger as expected (Bowman et al. 2018; Xu et al. 2021; Villanueva-Domingo et al. 2020; Cohen et al. 2017). The abnormal signal could be explained by many different schemes (Barkana 2018; Feng & Holder 2018; Yang 2018). On the other hand, the observational results of EDGES can be used to investigate the properties of DM (Clark et al. 2018; D'Amico et al. 2018; Yang 2018; Kovetz et al. 2019; Bhatt et al. 2019; Berlin et al. 2018; Barkana et al. 2018; Jia & Liao 2019; Hektor et al. 2018; Mittal et al. 2021; Chatterjee et al. 2019). The influence caused by the Hawking radiation from PBHs on the evolution of the IGM has

* Contact e-mail: ypyang@aliyun.com

been investigated, and then constraints on the abundance of PBHs has been obtained utilizing the EDGES results for $M_{\text{PBH}} \sim 10^{15} - 10^{17}$ g (Clark et al. 2018; Cang et al. 2021a). PBHs with masses $M_{\text{PBH}} \sim 10^{13} - 10^{14}$ g, whose lifetime is smaller than the present age of the Universe, have evaporated in the redshift range $z \sim 6 - 1100$. The observational results of EDGES can also be used to put upper limits on the initial mass fraction of these short-lived PBHs (Yang 2020; Halder & Banerjee 2021).

In theory, the global 21 cm signal appears in the epochs of reionization ($z \sim 6 - 10$), cosmic dawn ($z \sim 10 - 30$) and the dark ages ($z \sim 30 - 300$) (Furlanetto et al. 2006; Pritchard & Loeb 2012). In redshift $z \lesssim 30$, although the radiation from PBHs can effect the global 21 cm signal, the main effects come from the standard cosmological structures. Therefore, the dark ages is the best epoch for investigating the effects of PBHs. However, the frequency of the global 21 cm signal in the dark ages is redshifted to $\nu \lesssim 40$ MHz. The observation of these signals on the Earth is effected strongly by the Earth's ionosphere. Therefore, future radio telescopes on the Moon or satellites around a low Lunar orbit have been proposed (Burns et al. 2019, 2021; Burns 2020; Chen et al. 2019). In particular, for the Lunar farside, the influences from anthropogenic radio frequency interference can be mitigated. In this paper, we investigate the influences of the radiation from accreting PBHs on the evolution of the IGM and the global 21 cm signal in the dark ages. Then we discuss the possibilities of detecting accreting PBHs, combined with the expected observational ability of future experiments on the global 21 cm signal.

This paper is organized as follows. In Section 2 we discuss the basic properties of accreting PBHs. The influences of accreting PBHs on the evolution of IGM and the global 21 cm signal in the dark ages are investigated in Section 3. The relevant discussions and conclusions are given in Section 4 and 5, respectively.

2 THE BASIC PROPERTIES OF ACCRETING PBHs

The spherical accretion of matter on to a point mass was first researched by Hoyle & Lyttleton (1939, 1940b,a); Bondi & Hoyle (1944); Bondi (1952). An accretion disc could be formed if the accretion material has non-negligible angular momentum (Shapiro & Lightman 1976; Agol & Kamionkowski 2002; Poulin et al. 2017). Here we briefly review the basic properties of spherical accretion and give relevant discussions about disc accretion.

A PBH with mass M can accrete ambient baryonic matter at the Bondi-Hoyle rate \dot{M}_{HB} , which can be written as follows (Poulin et al. 2017):

$$\dot{M}_{\text{HB}} = 4\pi\lambda\rho_{\infty}\frac{(GM)^2}{v_{\text{eff}}^3}, \quad (1)$$

where G is the gravitational constant. $\rho_{\infty} = n_{\infty}m_p$ is the mass density far away from the PBH. m_p is the proton mass and n_{∞} is the mean cosmic gas density (Poulin et al. 2017; Ricotti et al. 2008):

$$n_{\infty} = 200 \text{ cm}^{-3} \left(\frac{1+z}{1000}\right)^3. \quad (2)$$

The accretion parameter λ takes into account the effects of gas viscosity, the Hubble expansion and the Compton scattering between the CMB and gas. Ricotti et al. (2008) have given a fitted formula of λ based on their analysis, which ignores the differences between low and high redshift ranges. A complete and detailed analysis is performed by Ali-Haïmoud & Kamionkowski (2017). They found a factor of ~ 10 decrease for λ at low redshift and we adopt their relevant results for our calculations. The effective velocity v_{eff} takes into account the gas sound speed far away from PBHs and the relative velocity between PBHs and baryons. The gas sound speed $c_{s,\infty}$ is in the form of (Poulin et al. 2017)

$$c_{s,\infty} = \sqrt{\frac{\gamma(1+x_e)T}{m_p}}, \quad (3)$$

where $\gamma = 5/3$ and x_e , T and m_p are the ionization fraction, the baryon temperature, and the proton mass, respectively. For the redshift range considered here, the gas sound speed $c_{s,\infty}$ can be approximated as follows (Poulin et al. 2017):

$$c_{s,\infty} \approx 6 \text{ km s}^{-1} \left(\frac{1+z}{1000}\right)^{1/2}. \quad (4)$$

In the linear regime, the square root of the variance of the relative velocity v_L is (Poulin et al. 2017; Ricotti et al. 2008)

$$\langle v_L^2 \rangle^{1/2} \approx \min \left[1, \frac{1+z}{1000} \right] \times 30 \text{ km s}^{-1}. \quad (5)$$

In the non-linear regime ($z \lesssim 30$), the relative velocity v_{NL} is different from that in the linear regime and can be approximated as $\langle v_{\text{NL}}^2 \rangle^{1/2} \approx 620 (1+z)^{-2.3} \text{ km s}^{-1}$ (Hasinger 2020). Because we will investigate the global 21 cm signal in the dark ages, therefore, the relative velocity v_L is used for our calculations. In order to investigate the energy injected into the IGM, one should average the luminosity of PBHs over the Gaussian distribution of relative velocities (Ali-Haïmoud & Kamionkowski 2017; Poulin et al. 2017; Ricotti et al. 2008). For this case, Ali-Haïmoud & Kamionkowski (2017) have proposed that the effective velocity is in the form of $v_{\text{eff}} \equiv \langle (c_{s,\infty}^2 + v_L^2)^{-3} \rangle^{-1/6}$ and can be approximated as follows:

$$v_{\text{eff}} \approx \begin{cases} \sqrt{c_{s,\infty} \langle v_L^2 \rangle^{1/2}} & \text{for } c_{s,\infty} \ll \langle v_L^2 \rangle^{1/2} \\ c_{s,\infty} & \text{for } c_{s,\infty} \gg \langle v_L^2 \rangle^{1/2} \end{cases} \quad (6)$$

The accretion luminosity of a PBH is proportional to the Bondi-Hoyle rate \dot{M}_{HB} (Poulin et al. 2017)

$$L_{\text{acc,PBH}} = \epsilon \dot{M}_{\text{HB}} c^2, \quad (7)$$

where ϵ is radiative efficiency. It depends on the details of the accretion and a typical value is $\epsilon = 0.01\dot{m}$ for spherical accretion (Ricotti et al. 2008). Ali-Haïmoud & Kamionkowski

(2017) reanalyzed the accretion process of PBHs and found an updated form for redshift $z \lesssim 500$:

$$\frac{\epsilon}{\dot{m}} \sim \begin{cases} 10^{-3} & \text{for photoionization} \\ 10^{-5} & \text{for collisional ionization} \end{cases} \quad (8)$$

where $\dot{m} = \dot{M}_{\text{HB}} c^2 / L_{\text{Edd}}$; $L_{\text{Edd}} = 1.26 \times 10^{38} (M/M_{\odot}) \text{ erg s}^{-1}$ is the Eddington luminosity. The energy injection rate per unit volume of accreting PBHs can be written as follows (Poulin et al. 2017):

$$\left(\frac{dE}{dV dt} \right)_{\text{PBH}} = L_{\text{acc, PBH}} f_{\text{pbh}} \frac{\rho_{\text{DM}}}{M_{\text{PBH}}}, \quad (9)$$

where $f_{\text{pbh}} = \rho_{\text{PBH}} / \rho_{\text{DM}}$. Here we have assumed a monochromatic mass function for PBHs. For the extended mass function, the energy injection rate per unit volume of accreting PBHs depends on the other parameters (Cang et al. 2021b).

3 THE EVOLUTION OF THE IGM AND GLOBAL 21 CM SIGNAL IN THE DARK AGES INCLUDING THE INFLUENCE OF ACCRETING PBHS

3.1 The evolution of the IGM including accreting PBHs

The evolution of the IGM is changed due to the effects of radiation from accreting PBHs. The main effects on the IGM are heating, ionization, and excitation (Zhang et al. 2007; Chen & Kamionkowski 2004; Clark et al. 2018; Yang 2019, 2015, 2018; Belotsky & Kirillov 2015). The changes of the ionization fraction (x_e) and the temperature of the IGM (T_k) with redshift are governed by following equations (Yang 2019, 2015; Chen & Kamionkowski 2004; Zhang et al. 2007):

$$(1+z) \frac{dx_e}{dz} = \frac{1}{H(z)} [R_s(z) - I_s(z) - I_{\text{PBH}}(z)], \quad (10)$$

$$(1+z) \frac{dT_k}{dz} = \frac{8\sigma_T a_R T_{\text{CMB}}^4 x_e (T_k - T_{\text{CMB}})}{3m_e c H(z) (1 + f_{\text{He}} + x_e)} - \frac{2}{3k_B H(z) (1 + f_{\text{He}} + x_e)} K_{\text{PBH}} + 2T_k, \quad (11)$$

where $R_s(z)$ and $I_s(z)$ are recombination and ionization rates respectively caused by the standard sources. I_{PBH} and K_{PBH} are the ionization and heating rates caused by accreting PBHs (Zhang et al. 2007; Chen & Kamionkowski 2004; Yang 2019; Clark et al. 2018; Yang 2015):

$$I_{\text{PBH}} = f(z) \frac{1}{n_b} \frac{1}{E_0} \times \left(\frac{dE}{dV dt} \right)_{\text{PBH}} \quad (12)$$

$$K_{\text{PBH}} = f(z) \frac{1}{n_b} \times \left(\frac{dE}{dV dt} \right)_{\text{PBH}} \quad (13)$$

where $f(z)$ stands for the energy fraction injected into the IGM for ionization, heating, and excitation, respectively. It

is a function of redshift and has been investigated in detail by e.g. Madhavacheril et al. (2014); Slatyer (2016). We have used the public code ExoCLASS (Stöcker et al. 2018), which is a branch of the public code CLASS (Blas et al. 2011), to calculate $f(z)$ (Poulin et al. 2017). In order to solve the differential equations mentioned above, we have followed the method used by e.g. Yang (2019, 2015, 2020); Chen & Kamionkowski (2004); Zhang et al. (2007); Clark et al. (2018), modifying the public code RECFAST in CAMB¹ to include the effects of radiation from accreting PBHs. The changes of x_e and T_k with redshift are shown in Fig. 1 (top and middle panels), where we also plot the fractional difference of x_e (T_k), defined as $\Delta x_e / x_e = (x_{e, \text{PBH}} - x_e) / x_e$, for accreting PBHs with $M_{\text{PBH}} = 10^3$ (10^4) M_{\odot} and $f_{\text{PBH}} = 10^{-1}$ (10^{-3}), respectively. For comparison, the standard case without accreting PBHs is also shown in Fig. 1 (dotted line). The top panel of Fig. 1 shows that the recombination is delayed due to the influence of accreting PBHs. At redshift $z \sim 100$, compared to the standard case, the ionization fraction x_e (the temperature of IGM T_k) increases about $\sim 150\%$ (30%) and $\sim 300\%$ (35%) respectively for the considered models of accreting PBHs.

3.2 The global 21 cm signal in the dark ages including accreting PBHs

The 21 cm line is related to the hyperfine transition between the triplet and singlet levels of the ground state of the hydrogen atom. With n_0 and n_1 as the number densities of hydrogen atoms in triplet and singlet states, the spin temperature T_s is defined as follows (Furlanetto et al. 2006; Pritchard & Loeb 2012):

$$\frac{n_1}{n_0} = 3 \exp\left(-\frac{0.068\text{K}}{T_s}\right). \quad (14)$$

The spin temperature is influenced by the background photons, the collisions between particles, and the resonant scattering of Ly α photons (Wouthuysen-Field effect) (Pritchard & Loeb 2012; Furlanetto et al. 2006). T_s is related to the temperature of the CMB (T_{CMB}) and IGM (T_k) as follows (Yuan et al. 2010; Cumberbatch et al. 2010):

$$T_s = \frac{T_{\text{CMB}} + (y_{\alpha} + y_c) T_k}{1 + y_{\alpha} + y_c}, \quad (15)$$

where y_{α} corresponds to the Wouthuysen-Field effect and we use the formula (Yuan et al. 2010; Yang 2019; Kuhlen et al. 2006)

$$y_{\alpha} = \frac{P_{10}}{A_{10}} \frac{0.068\text{K}}{T_k} e^{-0.3 \times (1+z)^{0.5} T_k^{-2/3} \left(1 + \frac{0.4}{T_k}\right)^{-1}}, \quad (16)$$

where $A_{10} = 2.85 \times 10^{-15} \text{ s}^{-1}$ is the Einstein coefficient of hyperfine spontaneous transition. P_{10} is the radiative de-excitation rate due to Ly α photons (Pritchard & Loeb 2012; Furlanetto et al. 2006). y_c is related to the collisions between hydrogen atoms and other particles (Yuan et al. 2010; Yang 2018; Kuhlen et al. 2006; Liszt 2001; Yang 2016),

¹ <https://camb.info/>

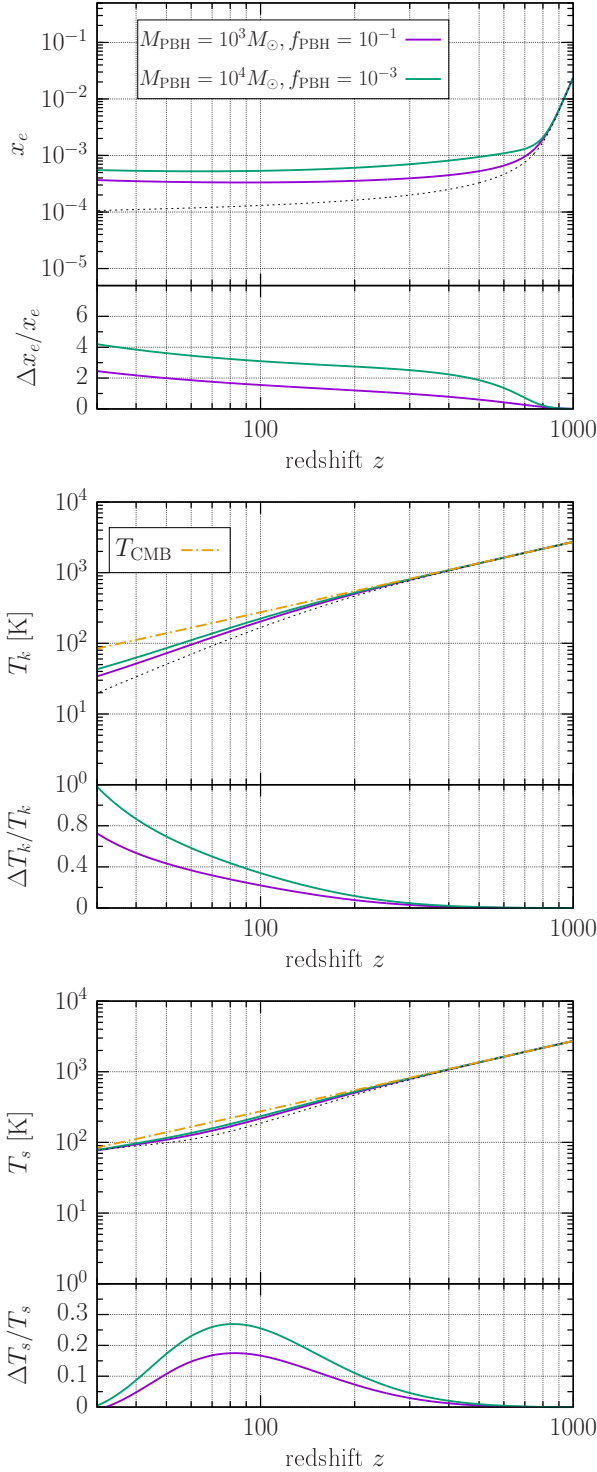


Figure 1. The changes of the ionization fraction (x_e , top panel), the gas temperature (T_k , middle panel), and the spin temperature (T_s , bottom panel) with redshift z for accreting PBH models with $M_{\text{PBH}} = 10^3(10^4) M_{\odot}$ and $f_{\text{PBH}} = 10^{-1}(10^{-3})$. The dotted line stands for the standard scenario without accreting PBHs. The fractional difference of x_e is defined as $\Delta x_e/x_e = (x_{e,\text{PBH}} - x_e)/x_e$ and the same definition is applied to T_k and T_s . Here we have set the radiative efficiency $\epsilon = 10^{-5}\dot{m}$, corresponding to the case of collisional ionization (Ali-Haïmoud & Kamionkowski 2017).

$$y_c = \frac{(C_{\text{HH}} + C_{\text{eH}} + C_{\text{pH}})0.068\text{K}}{A_{10}T_k}, \quad (17)$$

where $C_{\text{HH},\text{eH},\text{pH}}$ are the de-excitation rates and we adopt the fitted formulas used by Yang (2018, 2016); Kuhlen et al. (2006); Liszt (2001).

The differential brightness temperature, δT_b , relative to the CMB can be written as follows (Cumberbatch et al. 2010; Ciardi & Madau 2003; Yang 2018):

$$\delta T_b = 26(1 - x_e) \left(\frac{\Omega_b h}{0.02} \right) \left[\frac{1+z}{10} \frac{0.3}{\Omega_m} \right]^{\frac{1}{2}} \times \left(1 - \frac{T_{\text{CMB}}}{T_s} \right) \text{ mK}. \quad (18)$$

The variations of the spin temperature T_s with redshift are shown in the bottom panel of Fig. 1. We also plot the fractional difference in T_s , defined as $\Delta T_s/T_s = (T_{s,\text{PBH}} - T_s)/T_s$, for the considered models of accreting PBHs. T_s is decoupled with T_{CMB} at redshift $z \sim 600$ and coupled again at redshift $z \sim 30$. Including the influence of accreting PBHs, the maximum fractional difference appears at redshift $z \sim 80$ and the degree of difference depends on the specific model of accreting PBHs.

In the top panel of Fig. 2, we show the evolution of the differential brightness temperature δT_b with redshift z . As shown in Fig. 1, compared to the standard scenario, the spin temperature T_s increases in the redshift range $z \sim 30 - 400$ for the case of accreting PBHs. Since the differential brightness temperature δT_b is proportional to $(1 - T_{\text{CMB}}/T_s)$, the amplitude of δT_b is decreased as shown in Fig. 2. In addition, we also show the brightness temperature deviation, $\Delta \delta T_b = \delta T_{b,\text{PBH}} - \delta T_b$, of the considered accreting PBHs models from the standard scenario (dotted line). The deviation $\Delta \delta T_b$ achieves the maximum value ~ 18 (26) mK at redshift $z \sim 90$ for accreting PBHs with $M_{\text{PBH}} = 10^3$ (10^4) M_{\odot} and $f_{\text{PBH}} = 10^{-1}$ (10^{-3}).

The gradient of the differential brightness temperature, $d\delta T_b/d\nu$, is shown in the bottom panel of Fig. 2, where the dotted line stands for the standard case. For the standard case, $d\delta T_b/d\nu$ achieves ~ 1.8 mK MHz $^{-1}$ at the frequency $\nu \sim 28$ MHz ($z \sim 50$). Including the effects of accreting PBHs, in the frequency range of $\nu \sim 20 - 40$ MHz, the amplitude of $d\delta T_b/d\nu$ is reduced, $\lesssim 1$ mK MHz $^{-1}$ for the considered models of accreting PBHs.

4 DISCUSSIONS

Since the frequency of the global 21 cm signal in the dark ages is redshifted to $\nu \lesssim 40$ MHz and the Earth's ionosphere has a strong influence on the detection of these signals, it is impossible to detect these radio signals from the Earth. It has been proposed that the radio telescope, either in lunar orbit or on the farside surface of the Moon, could detect the global 21 cm signal of the dark ages (Burns et al. 2019, 2021; Burns 2020; Chen et al. 2019). Burns et al. (2019) argued that a future radio telescope can detect the differential brightness temperature of the global 21 cm signal in the dark ages with 1σ uncertainty of $\delta T_b \sim 15$ mK, depending on the observation time. For accreting PBHs with mass $M_{\text{PBH}} = 10^3 M_{\odot}$ and mass fraction $f_{\text{PBH}} = 10^{-1}$, the brightness temperature deviation $\Delta \delta T_b$ reaches ~ 18 mK at the

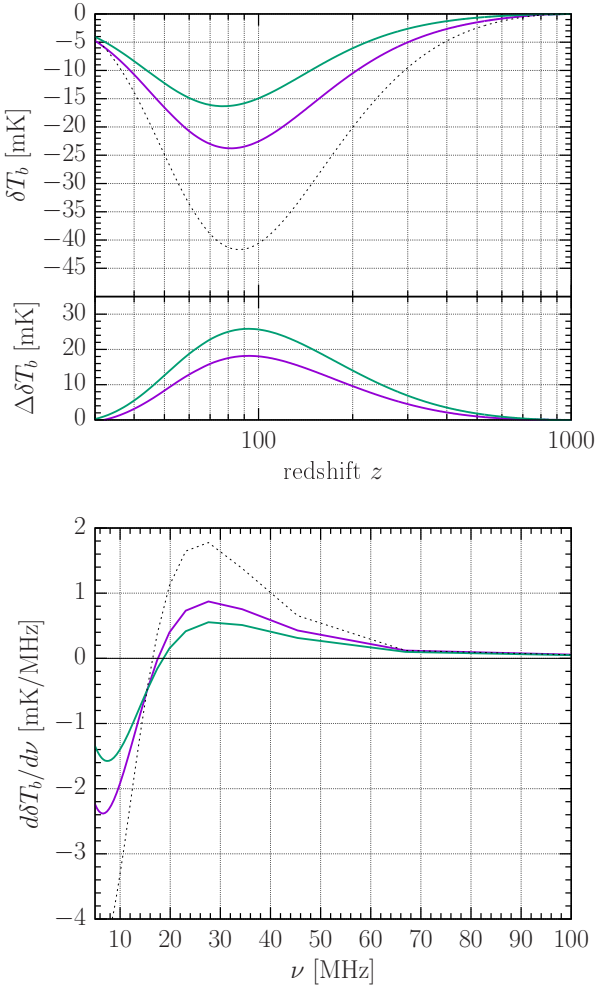


Figure 2. *Top panel.* The changes of the brightness temperature deviation, $\Delta\delta T_b = \delta T_{b,\text{PBH}} - \delta T_b$, with redshift z for accreting PBH models same as in Fig. 1. *Bottom panel.* The gradient of the differential brightness temperature $d\delta T_b/d\nu$ as a function of frequency ν . The line style is the same as in Fig. 1.

frequency $\nu \sim 16$ MHz. At the same frequency, the deviation $\Delta\delta T_b$ is up to ~ 26 mK for $M_{\text{PBH}} = 10^4 M_\odot$ and $f_{\text{PBH}} = 10^{-3}$. Therefore, it is expected that future extraterrestrial radio telescope will have the ability to distinguish the accreting PBHs model from the standard model, especially for larger PBHs with higher mass fraction.

For the geometry of gas accretion on to PBHs, we have considered the conservative case of spherical accretion but not disc accretion. The formation of an accretion disc and its impacts on the anisotropy of CMB have been discussed by e.g. Poulin et al. (2017); Ricotti et al. (2008). A thin disc around a PBH could be formed for $\dot{m} > 1$ and the radiative efficiency ϵ is about $\sim 0.06 - 0.4$ (Ricotti et al. 2008). For the scenario considered here, the accretion rate is $\dot{m} < 1$ and a thick disc could be formed if the accreting gas has non-negligible angular momentum. In this case, an advection dominated accretion flow (Yuan & Narayan 2014) can be formed and the radiative efficiency is about a factor of 10 larger than that of spherical accretion (Ricotti et al. 2008). As a result, in the disc accretion scenario x_e, T_k , and T_s will be increased compared to the case of spherical accre-

tion for the same mass and mass fraction of PBHs. It is also expected that the amplitude of absorption trough ($|\delta T_b|$) of the global 21 cm signal in the dark ages becomes smaller, and the brightness temperature deviation $\Delta\delta T_b$ becomes larger for the disc accretion scenario. In Fig. 3, a comparison between the cases of spherical accretion and disc accretion is shown for $M_{\text{PBH}} = 10^3 M_\odot$ and $f_{\text{PBH}} = 10^{-1}$. For disc accretion, we have set the accretion parameter $\lambda = 0.01$ and the radiative efficiency $\epsilon = 0.1\dot{m}$, corresponding to the benchmark model used by Poulin et al. (2017) for investigating the effects on the CMB. For this case, emission signals appear in the redshift range $z \sim 30 - 100$. The brightness temperature deviation $\Delta\delta T_b$ reaches ~ 48 mK at the frequency $\nu \sim 18$ MHz ($z \sim 80$). The gradient of the differential brightness temperature $d\delta T_b/d\nu$ achieves ~ 0.8 mK MHz $^{-1}$ at the frequency $\nu \sim 14$ MHz ($z \sim 100$).

The mass fraction of PBHs has been constrained by different astrophysical observations (for a recent review see e.g. Carr et al. (2020)). Poulin et al. (2017) used the Planck data to get the upper limits on the mass fraction of PBHs. They found that for $M_{\text{PBH}} = 10^3 M_\odot$ the limits are $f_{\text{PBH}} \lesssim 10^{-2}$ ($\lesssim 10^{-4}$) for spherical accretion (disc accretion). In Fig. 4, we show the brightness temperature deviation $\Delta\delta T_b$ for different mass fraction of PBHs with $M_{\text{PBH}} = 10^3 M_\odot$ for disc accretion. For $f_{\text{PBH}} \sim 10^{-4}$, the maximum deviation is ~ 1 mK at redshift $z \sim 85$ ($\nu \sim 17$ MHz). This is smaller than the 1σ uncertainty of $\delta T_b \sim 5$ mK, which could be achieved by $\sim 10^5$ hours observation with a future radio telescope (Burns 2020; Rapetti et al. 2020). The brightness temperature deviation $\Delta\delta T_b$ reaches ~ 8 mK at redshift $z \sim 85$ for $f_{\text{PBH}} \sim 10^{-3}$. It can also be seen that for $f_{\text{PBH}} \sim \text{few} \times 10^{-3} - 10^{-2}$, at the redshift range $z \sim 50 - 100$, the brightness temperature deviation can be larger than the 1σ uncertainty of $\delta T_b \sim 15$ mK, which could be achieved by ~ 20000 hours observation with a future radio telescope (Burns 2020; Rapetti et al. 2020).²

In Fig. 5, the expected upper limits on f_{PBH} are shown for future detection of the global 21 cm signal in the dark ages (red solid line, labelled 'dark ages'). The constraints are obtained by requiring $\delta T_b \lesssim -37$ mK, which corresponds to 5 mK uncertainty of the largest amplitude of the global 21 cm signal ($\delta T_b \sim -42$ mK) in the dark ages. For comparison, constraints from a few other studies are also shown: 1) constraints from the global 21 cm signal in the cosmic dawn reported by the Experiment to Detect the Global Epoch of Reionization Signature (EDGES) (Hektor et al. 2018) (brown dashed line, labelled 'EDGES'); 2) the expected constraints from the 21 cm power spectrum in the cosmic dawn, which could be detected by e.g. the Hydrogen Epoch of Reionization Array (HERA) (Mena et al. 2019) (black dashed line, labelled 'HERA'); 3) upper limits from the CMB data observed by Planck (Poulin et al. 2017) (blue dashed line, labelled 'Planck'); 4) constraints from the studies of the effects of PBHs on the dynamical evolution of stars in dwarf galaxy Segue I (Koushiappas & Loeb 2017) (green dashed line, labelled 'Segue I'); 5) non-detection of the stochastic gravita-

² Here we neglect the frequency dependence of uncertainty and one can refer to Rapetti et al. (2020) for more detailed discussions.

tional wave background by LIGO (Raidal et al. 2017) (magenta line, labelled 'LIGO'); 6) constraints from the investigation of the number density of X-ray objects in galaxies (Inoue & Kusenko 2017) (orange line, labelled 'X-ray'). Compared with the constraints from LIGO, the upper limits from the dark ages are stronger for the mass range of $300 \lesssim M_{\text{PBH}} \lesssim 10^4 M_{\odot}$. Similar cases with a slightly different mass range can also be found for EDGES, Planck, X-ray, and Segue I. As shown in Fig. 5, future detection of the 21 cm power spectrum by e.g. HERA could provide the strongest constraints for the mass range considered here. Although the constraints from the dark ages is not the strongest, as mentioned above, since the astrophysical environment of the dark ages is relatively clean, future detection of the global 21 cm signal in the dark ages is still very useful for the studies of PBHs. Note that there are many works investigating the constraints on the mass fraction of PBHs not shown in Fig. 5, and one can refer to e.g. Carr et al. (2020) for a recent review.

For our calculations, we have considered the gas accretion on to 'naked' PBHs. If PBHs do not make up all dark matter, they should also accrete dark matter particles around them forming 'clothed' PBHs (Ricotti et al. 2008; De Luca et al. 2020; Cai et al. 2021; Ricotti 2007). The accretion rate of 'clothed' PBHs is larger than that of 'naked' PBHs (Ricotti et al. 2008). Therefore, compared with the case of 'naked' PBHs, the brightness temperature deviation of the global 21 cm signal in the dark ages should be larger for the case of 'clothed' PBHs for the same mass and mass fraction of PBHs.

For the calculations above, we have set the radiative efficiency $\epsilon = 10^{-5} \dot{m}$, corresponding to the case of collisional ionization (Ali-Haïmoud & Kamionkowski 2017). For photoionization the radiative efficiency is about two orders of magnitude larger (Eq. 8). Therefore, the brightness temperature deviation of the global 21 cm signal in the dark ages should be larger for the case of photoionization than that of collisional ionization for the same mass and mass fraction of PBHs.

5 CONCLUSIONS

We have investigated the influences of accreting PBHs on the global 21 cm signal in the dark ages. By taking into account the benchmark model (spherical accretion) of accreting PBHs with mass $M_{\text{PBH}} = 10^3$ (10^4) M_{\odot} and mass fraction $f_{\text{PBH}} = 10^{-1}$ (10^{-3}), we found that the maximum brightness temperature deviation of the global 21 cm signal, $\Delta\delta T_b$, reaches ~ 18 (26) mK at redshift $z \sim 90$, corresponding to the frequency $\nu \sim 16$ MHz. The gradient of the differential brightness temperature $d\delta T_b/d\nu$ is ~ 0.8 (0.5) mK MHz^{-1} for the models considered. For larger PBHs with higher mass fraction, the brightness temperature deviation is larger in the redshift range of $z \sim 30 - 300$ ($\nu \sim 5 - 46$ MHz) and the gradient is lower in the frequency range $\nu \sim 20 - 40$ MHz ($z \sim 35 - 70$). In addition, an accretion disc can be formed around PBHs if the accreting gas has non-negligible angular momentum. Due to the higher radiative efficiency in the disc accretion scenario, the brightness temperature deviation and the gradient of the global 21 cm signal are larger than those of spherical accretion.

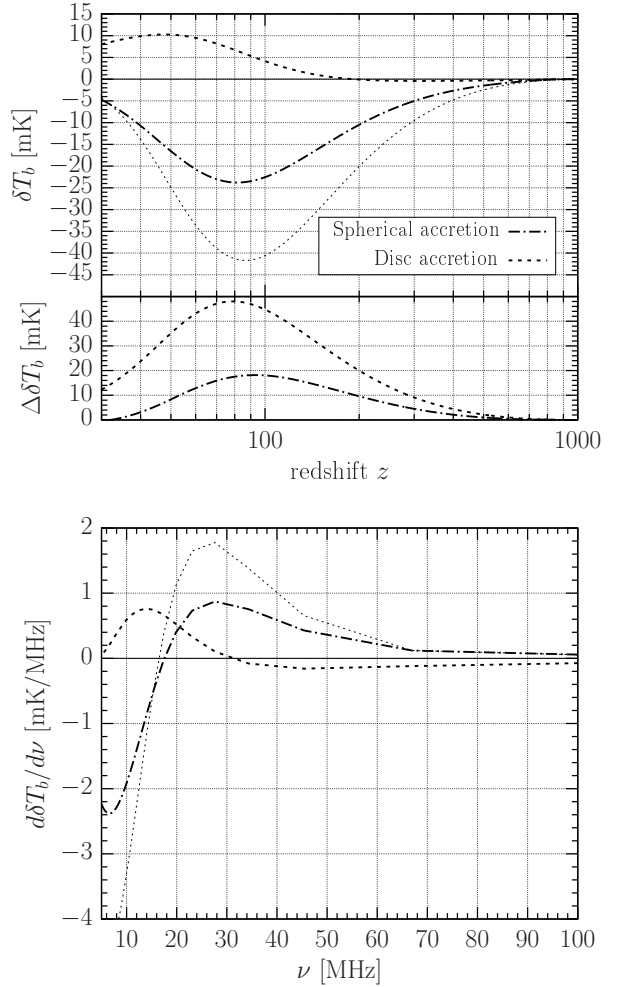


Figure 3. The comparison between the cases of spherical accretion (dot-dashed line) and disk accretion (dashed line) for $M_{\text{PBH}} = 10^3 M_{\odot}$ and $f_{\text{PBH}} = 10^{-1}$. For disk accretion, we have set the accretion parameter $\lambda = 0.01$ and the radiative efficiency $\epsilon = 0.1 \dot{m}$. *Top panel.* The changes of the brightness temperature deviation, $\Delta\delta T_b = \delta T_{b,\text{PBH}} - \delta T_b$, with redshift z . *Bottom panel.* The gradient of the differential brightness temperature $d\delta T_b/d\nu$ as a function of frequency ν .

Due to the influences of the Earth's ionosphere, it is impossible to detect the global 21 cm signal in the dark ages from the Earth. Future radio telescopes in lunar orbit or on the farside surface of the Moon, where the uncertainty of detecting the brightness temperature of the global 21 cm signal could reach at least ~ 15 mK, could have the ability to distinguish the global 21 cm signal impacted by accreting PBHs from that of the standard scenario. On the other hand, detection of the gradient of the differential brightness temperature in the frequency range $\nu \sim 20 - 40$ MHz with a amplitude smaller than ~ 1.8 mK MHz^{-1} will provide a possible evidence of accreting PBHs.

6 ACKNOWLEDGEMENTS

Y. Yang thanks Dr. Bin Yue and Fupeng Zhang for useful discussions. We thank an anonymous referee for useful

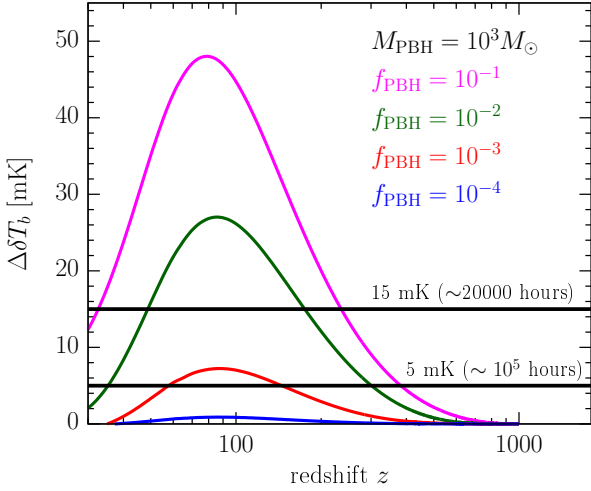


Figure 4. The brightness temperature deviation $\Delta\delta T_b$ for different mass fraction of PBHs with $M_{\text{PBH}} = 10^3 M_{\odot}$ for the disk accretion scenario. The horizontal lines show the uncertainty of δT_b (1σ), 5 mK and 15 mK, which could be achieved by $\sim 10^5$ and ~ 20000 hours observation of future radio telescope (Burns 2020; Rapetti et al. 2020).

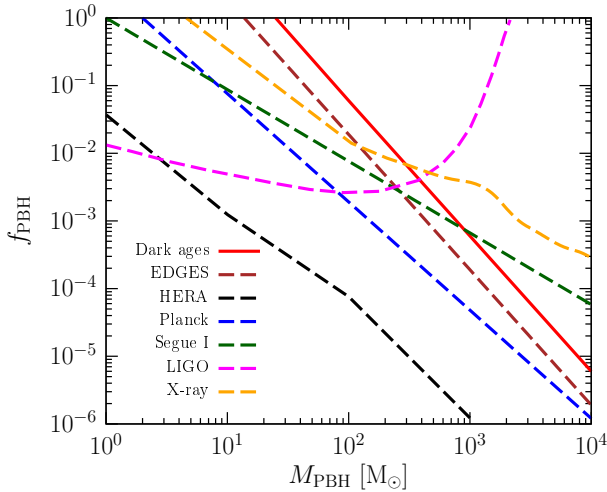


Figure 5. Upper limits on the mass fraction of PBHs for future observation of the 21 cm signal in the dark ages for the disk accretion scenario (red solid line, labelled dark ages). For comparison, the constraints from a few other studies are also shown (dashed lines in different colors): 1) constraints from the observation of the global 21 cm signal in the cosmic dawn by EDGES (brown line, labelled 'EDGES') (Hektor et al. 2018); 2) future detection of the 21 cm power spectrum in the cosmic dawn by HERA (black line, labelled 'HERA') (Mena et al. 2019); 3) constraints from the CMB using the Planck data (blue line, labelled 'Panck') (Poulin et al. 2017); 4) the influences of PBHs on the dynamical evolution of stars in dwarf galaxy Segue I (green line, labelled 'Segue I') (Koushiappas & Loeb 2017); 5) non-detection of the stochastic GW background by LIGO (magenta line, labelled 'LIGO') (Raidal et al. 2017); 6) investigation of the number density of X-ray objects in galaxies (orange line, labelled 'X-ray') (Inoue & Kusenko 2017). Note that the region above each line is excluded by the corresponding study.

comments and suggestions. Y. Yang thanks Hao Jiao and Shikhar Mittal for useful comments. Y. Yang is supported in part by the Youth Innovations and Talents Project of Shandong Provincial Colleges and Universities (Grant No. 201909118)

7 DATA AVAILABILITY

No new data were generated or analysed in support of this research.

REFERENCES

- Agol E., Kamionkowski M., 2002, *Mon. Not. Roy. Astron. Soc.*, 334, 553
- Ali-Haïmoud Y., Kamionkowski M., 2017, *Phys. Rev.*, D95, 043534
- Barkana R., 2018, *Nature*, 555, 71
- Barkana R., Outmezguine N. J., Redigolo D., Volansky T., 2018, *Phys. Rev.*, D98, 103005
- Belotsky K. M., Kirillov A. A., 2015, *JCAP*, 1501, 041
- Berlin A., Hooper D., Krnjaic G., McDermott S. D., 2018, *Phys. Rev. Lett.*, 121, 011102
- Bertone G., Hooper D., Silk J., 2005, *Phys. Rept.*, 405, 279
- Bhatt J. R., Mishra A. K., Nayak A. C., 2019, *Phys. Rev.*, D100, 063539
- Bird S., Cholis I., Muñoz J. B., Ali-Haïmoud Y., Kamionkowski M., Kovetz E. D., Raccanelli A., Riess A. G., 2016, *Phys. Rev. Lett.*, 116, 201301
- Blas D., Lesgourgues J., Tram T., 2011, *Journal of Cosmology and Astroparticle Physics*, 2011, 034
- Bondi H., 1952, *Mon. Not. Roy. Astron. Soc.*, 112, 195
- Bondi H., Hoyle F., 1944, *Mon. Not. Roy. Astron. Soc.*, 104, 273
- Bowman J. D., Rogers A. E. E., Monsalve R. A., Mozdzen T. J., Mahesh N., 2018, *Nature*, 555, 67
- Burns J. O., 2020, *Phil. Trans. R. Soc. A.*, 379, 20190564
- Burns J., et al., 2019, *BAAS*, 51, 6
- Burns J., et al., 2021, arXiv e-prints, p. arXiv:2103.05085
- Cai R.-G., Ding Y.-C., Yang X.-Y., Zhou Y.-F., 2021, *J. Cosmology Astropart. Phys.*, 2021, 057
- Cang J., Gao Y., Ma Y.-Z., 2021a, arXiv e-prints, p. arXiv:2108.13256
- Cang J., Gao Y., Ma Y.-Z., 2021b, *J. Cosmology Astropart. Phys.*, 2021, 051
- Carr B. J., Kohri K., Sendouda Y., Yokoyama J., 2010, *Phys. Rev. D*, 81, 104019
- Carr B., Kohri K., Sendouda Y., Yokoyama J., 2020, arXiv e-prints, p. arXiv:2002.12778
- Chatterjee A., Dayal P., Choudhury T. R., Hutter A., 2019, *MNRAS*, 487, 3560
- Chen X., Kamionkowski M., 2004, *Phys. Rev. D*, 70, 043502
- Chen X., et al., 2019, in *ISSI-BJ Forum: Discover the Sky by Longest Wavelength with Small Satellite Constellation* (arXiv:1907.10853)
- Ciardi B., Madau P., 2003, *Astrophys. J.*, 596, 1
- Clark S., Dutta B., Gao Y., Ma Y.-Z., Strigari L. E., 2018, *Phys. Rev.*, D98, 043006
- Cohen A., Fialkov A., Barkana R., Lotem M., 2017, *Mon. Not. Roy. Astron. Soc.*, 472, 1915
- Cumberbatch D. T., Lattanzi M., Silk J., Lattanzi M., Silk J., 2010, *Phys. Rev.*, D82, 103508
- D'Amico G., Panci P., Strumia A., 2018, *Phys. Rev. Lett.*, 121, 011103

- De Luca V., Franciolini G., Pani P., Riotto A., 2020, *Phys. Rev. D*, 102, 043505
- De Luca V., Franciolini G., Riotto A., 2021a, *Phys. Rev. Lett.*, 126, 041303
- De Luca V., Desjacques V., Franciolini G., Pani P., Riotto A., 2021b, *Phys. Rev. Lett.*, 126, 051101
- Feng C., Holder G., 2018, *Astrophys. J.*, 858, L17
- Furlanetto S., Oh S. P., Briggs F., 2006, *Phys. Rept.*, 433, 181
- Halder A., Banerjee S., 2021, *Phys. Rev. D*, 103, 063044
- Hasinger G., 2020, *JCAP*, 07, 022
- Hektor A., Hütsi G., Marzola L., Raidal M., Vaskonen V., Veermäe H., 2018, *Phys. Rev.*, D98, 023503
- Hoyle F., Lyttleton R. A., 1939, *Math. Proc. Cambridge Philos. Soc.*, 35, 405
- Hoyle F., Lyttleton R. A., 1940a, *Math. Proc. Cambridge Philos. Soc.*, 36, 325
- Hoyle F., Lyttleton R. A., 1940b, *Math. Proc. Cambridge Philos. Soc.*, 36, 424
- Inoue Y., Kusenko A., 2017, *JCAP*, 1710, 034
- Jia L.-B., Liao X., 2019, *Phys. Rev. D*, 100, 035012
- Jungman G., Kamionkowski M., Griest K., 1996, *Phys. Rept.*, 267, 195
- Kohri K., Terada T., 2021, *Phys. Lett. B*, 813, 136040
- Koushiappas S. M., Loeb A., 2017, *Phys. Rev. Lett.*, 119, 041102
- Kovetz E. D., Cholis I., Kaplan D. E., 2019, *Phys. Rev.*, D99, 123511
- Kuhlen M., Madau P., Montgomery R., 2006, *Astrophys. J.*, 637, L1
- Liszt H., 2001, *Astron. Astrophys.*, 371, 698
- Madhavacheril M. S., Sehgal N., Slatyer T. R., 2014, *Phys. Rev.*, D89, 103508
- Mena O., Palomares-Ruiz S., Villanueva-Domingo P., Witte S. J., 2019, *Phys. Rev.*, D100, 043540
- Mittal S., Ray A., Kulkarni G., Dasgupta B., 2021, arXiv e-prints, p. [arXiv:2107.02190](https://arxiv.org/abs/2107.02190)
- Page D. N., 1976a, *Phys. Rev. D*, 13, 198
- Page D. N., 1976b, *Phys. Rev. D*, 14, 3260
- Page D. N., 1977, *Phys. Rev. D*, 16, 2402
- Poulin V., Serpico P. D., Calore F., Clesse S., Kohri K., 2017, *Phys. Rev.*, D96, 083524
- Pritchard J. R., Loeb A., 2012, *Rept. Prog. Phys.*, 75, 086901
- Raidal M., Vaskonen V., Veermäe H., 2017, *JCAP*, 09, 037
- Rapetti D., Tauscher K., Mirocha J., Burns J. O., 2020, *ApJ*, 897, 174
- Ricotti M., 2007, *Astrophys. J.*, 662, 53
- Ricotti M., Ostriker J. P., Mack K. J., 2008, *Astrophys. J.*, 680, 829
- Shapiro S. L., Lightman A. P., 1976, *ApJ*, 204, 555
- Slatyer T. R., 2016, *Phys. Rev.*, D93, 023521
- Stöcker P., Krämer M., Lesgourgues J., Poulin V., 2018, *JCAP*, 1803, 018
- Tashiro H., Sugiyama N., 2013, *Mon. Not. Roy. Astron. Soc.*, 435, 3001
- Ünal C., Kovetz E. D., Patil S. P., 2021, *Phys. Rev. D*, 103, 063519
- Villanueva-Domingo P., Ichiki K., 2021, arXiv e-prints, p. [arXiv:2104.10695](https://arxiv.org/abs/2104.10695)
- Villanueva-Domingo P., Mena O., Miralda-Escudé J., 2020, *Phys. Rev. D*, 101, 083502
- Xu Y., Yue B., Chen X., 2021, arXiv e-prints, p. [arXiv:2102.12865](https://arxiv.org/abs/2102.12865)
- Yang Y., 2015, *Phys. Rev.*, D91, 083517
- Yang Y., 2016, *Eur. Phys. J. Plus*, 131, 432
- Yang Y., 2018, *Phys. Rev.*, D98, 103503
- Yang Y., 2019, *Mon. Not. Roy. Astron. Soc.*, 486, 4569
- Yang Y., 2020, *Phys. Rev. D*, 102, 083538
- Yuan F., Narayan R., 2014, *Ann. Rev. Astron. Astrophys.*, 52, 529
- Yuan Q., Yue B., Bi X.-J., Chen X., Zhang X., 2010, *JCAP*, 1010, 023
- Zhang L., Chen X., Kamionkowski M., Si Z.-g., Zheng Z., 2007, *Phys. Rev. D*, 76, 061301